Pressure-Dependent Optical and Vibrational Properties of Monolayer Molybdenum Disulfide

Avinash P. Nayak[1‡], Tribhuwan Pandey[2‡], Damien Voiry[3], Jin Liu[4], Samuel T. Moran[1], Ankit Sharma[1], Cheng Tan[1], Chang-Hsiao Chen[6], Lain-Jong Li[7], Manish Chhowalla[3], Jung-Fu Lin[4,5], Abhishek K. Singh[2], Deji Akinwande[1]**

SUPPLEMENTARY INFORMATION

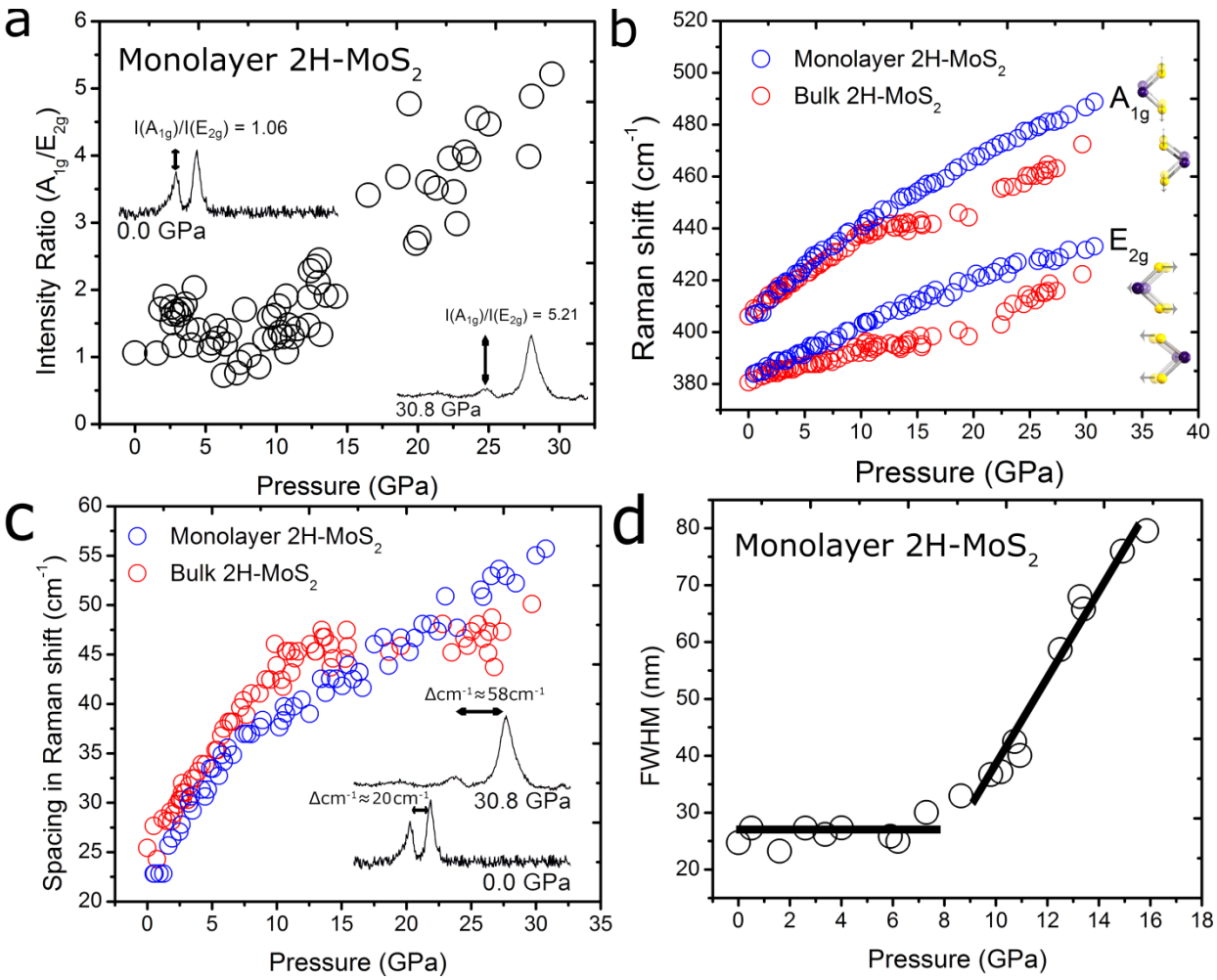

Figure S1. Vibrational and Optical Properties of Bulk and Monolayer 2H-MoS_2 at High Pressures. **(a)** Intensity ratio of the A_{1g} and E_{2g} peaks. The E_{2g} mode is observed to diminish in comparison to the A_{1g}. The insets show the relative intensities of the E_{2g} and A_{1g} peaks at selected pressures. (**b**) Pressure dependence of the Raman frequencies of the A_{1g} and the E_{2g} modes as a function of pressure. The behavior of these vibrational Raman modes in monolayer 2H-MoS_2 at high pressures (blue circles) deviates significantly from that of the bulk counterpart (red circles) due to the absence of interlayer interactions. Inset: representative vibrations involved in A_{1g} and E_{2g} modes. The A_{1g} modes originate from transverse vibrations of S-S atom, however the E_{2g} mode emerges from longitudinal vibrations of Mo and S atoms in opposite directions. (**c**) Raman frequency separation between the A_{1g} and E_{2g} peak as 1) a function of pressure for monolayer and bulk 2H-MoS_2. Inset: representative Raman spectra highlighting the separation at 0 GPa and 30.8 GPa. The in-plane A_{1g} mode becomes more dominant in intensity than the E_{2g} past ~16 GPa for the monolayer 2H-MoS_2. **(d)** PL FWHM with pressure up to 16 GPa. The black lines serves as visual guidelines.

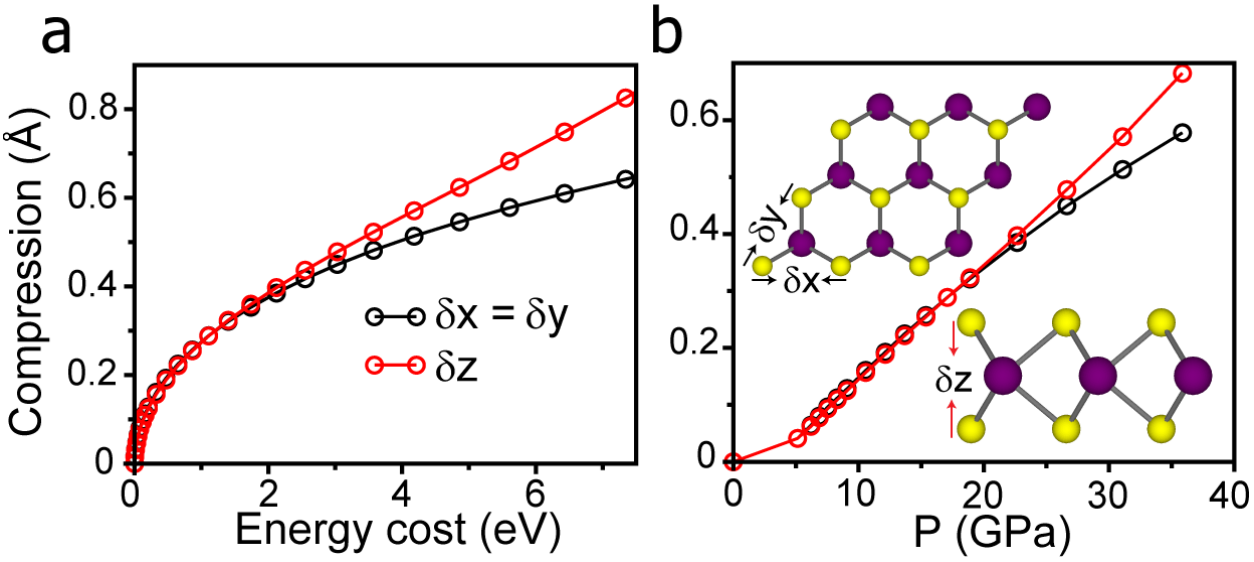

Figure S2. Modeling of hydrostatic pressure on monolayer MoS_2. (a) Compression of atoms plotted with respect to energy required to compress the in-plane (*x*, *y*) and out of plane (*z*) bonds. **(b)** Compression of atoms is plotted with respect to pressure. Till 20 GPa pressure there is equal compression in all the three direction. After 18 GPa. Compression along the *z* direction becomes more favorable. Inset: Schematic representing the compression of atoms in the in-plane direction (upper inset) and out-of-plane directions

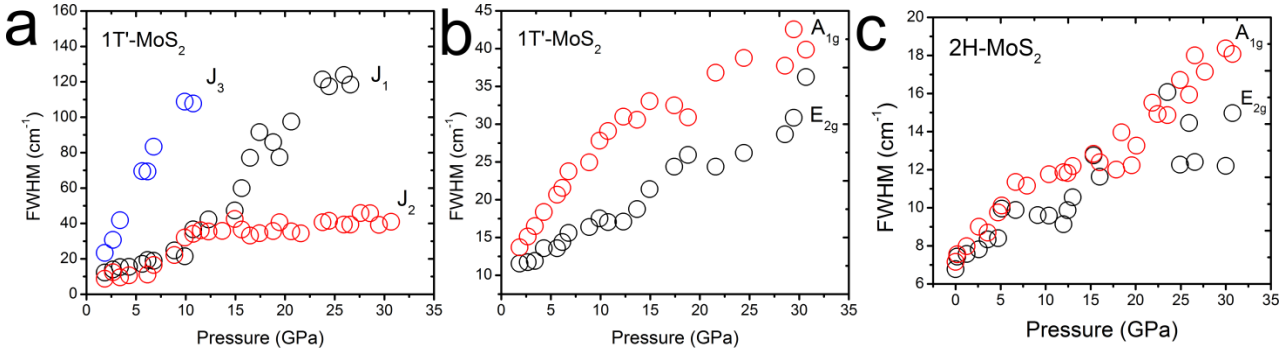

Figure S3. Raman Spectroscopic Results of Restacked 1T'-MoS_2 and monolayer 2H-MoS_2 at High Pressures. (a) FWHM of J_1, J_2 and J_3 Raman modes. The J_3 mode tends to saturate at 10 GPa while J_2 and J_3 increase in FWHM. **(b)** The FWHM of the E_{2g} and A_{1g} increases with pressure. **(c)** The FWHM of the E_{2g} and A_{1g} Raman modes for 2H-MoS_2. The FWHM is notably smaller for the 2H-MoS_2 monolayer than the 1T'-MoS_2 since the J_3 mode merges with the E_{2g} mode.

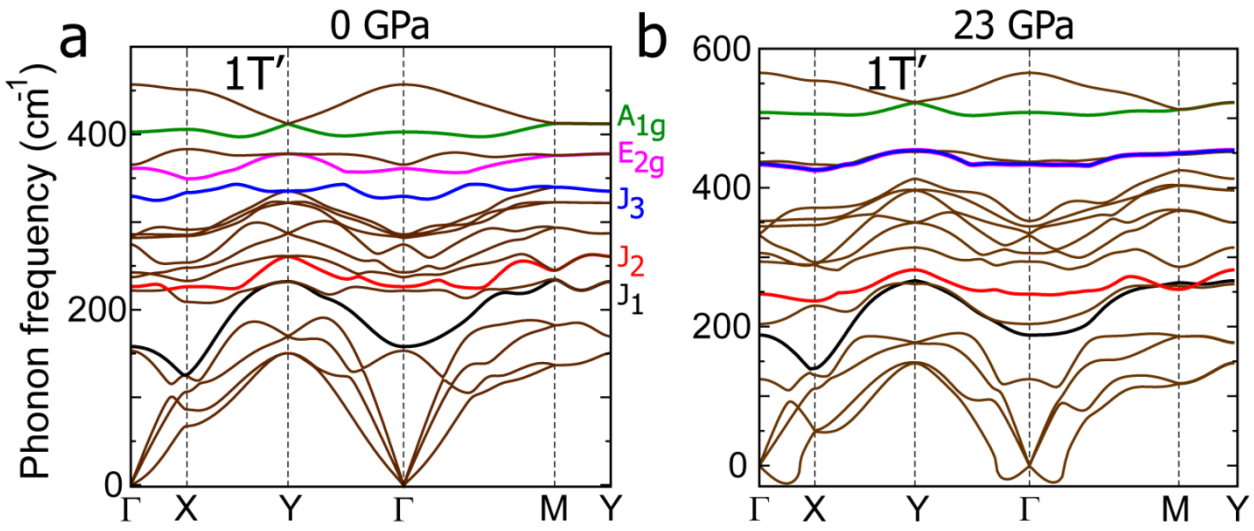

Figure S4. Phonon Dispersions for Monolayer 1T'-MoS_2 at Representative Pressures. The Raman active modes for 1T'-MoS_2 are highlighted with different colors for clarity at **(a)** 0 GPa and **(b)** 23 GPa. The Raman active A_{1g}, E_{2g}, J_1, J_2 and J_3 modes are identified from the dispersion curves at the Γ point. As can be seen in case of 1T'-MoS_2 three new modes J_1, J_2 and J_3 appear, whereas the frequency of the E_{2g} mode decreases significantly compared to bulk MoS_2. The J_3 mode merges with the E_{2g} mode at ~10 GPa.

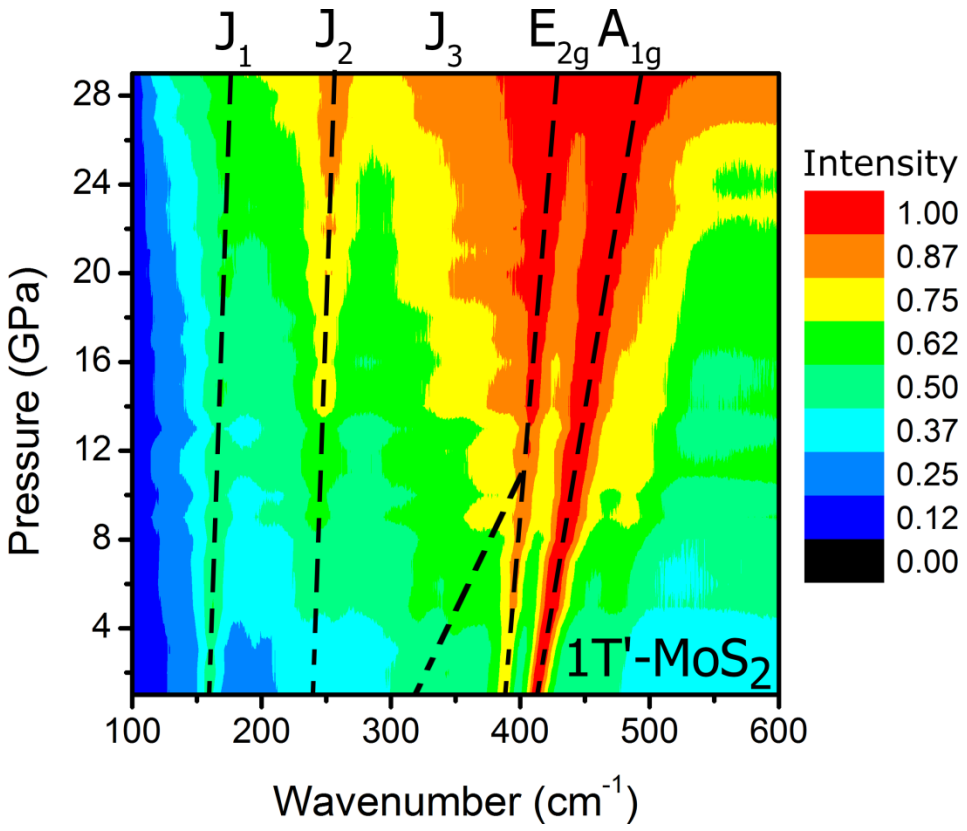

Figure S5. **Raman Intensity Map of 1T'-MoS_2.** The pressure dependent Raman shows the shift and broadening of the 1T'-MoS_2 Raman active modes. The dominant Raman active modes at high pressure are J_2, E_{2g}, and A_{1g}.

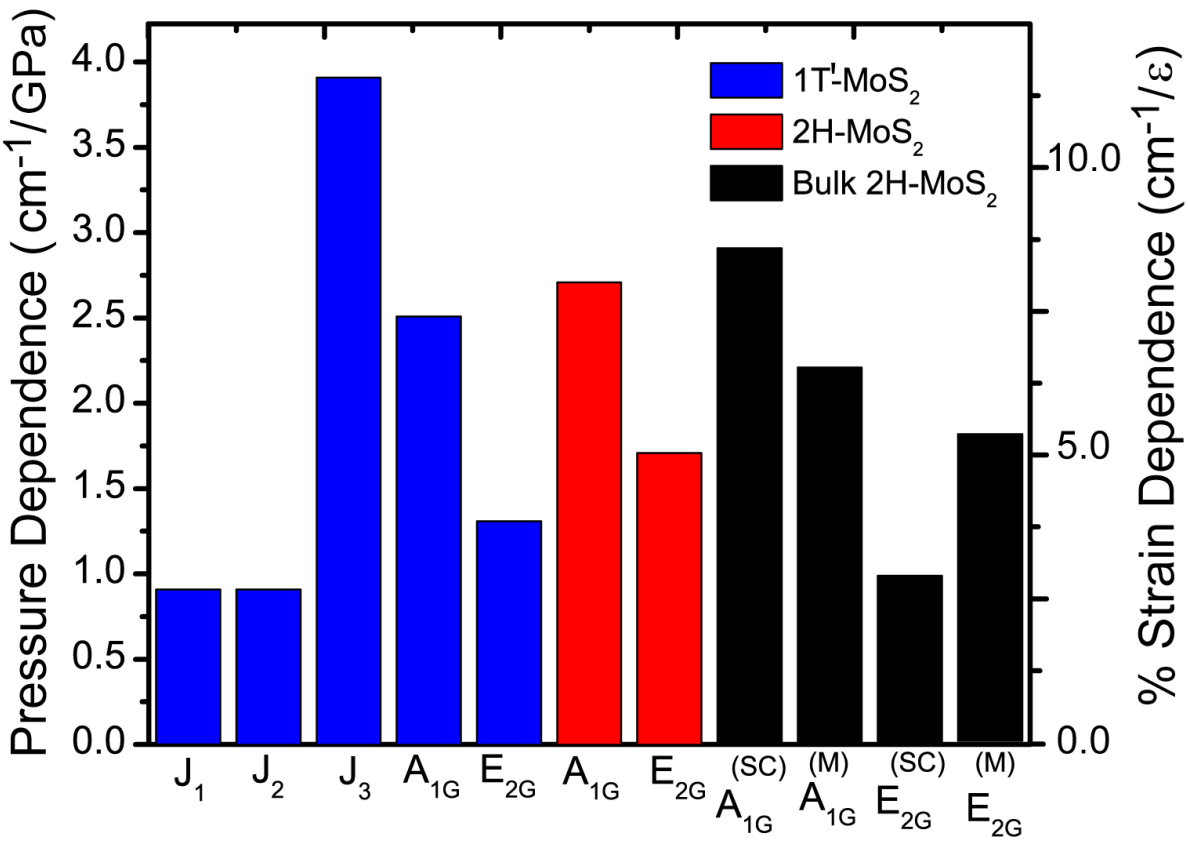

Figure S6. Raman Shift with Pressure. The pressure dependence of the Raman modes for the monolayer 2H and 1T'-MoS_2 polytypes compared to the bulk 2H-MoS_2 analog in their semiconducting (SC) and metallic (M) regime.

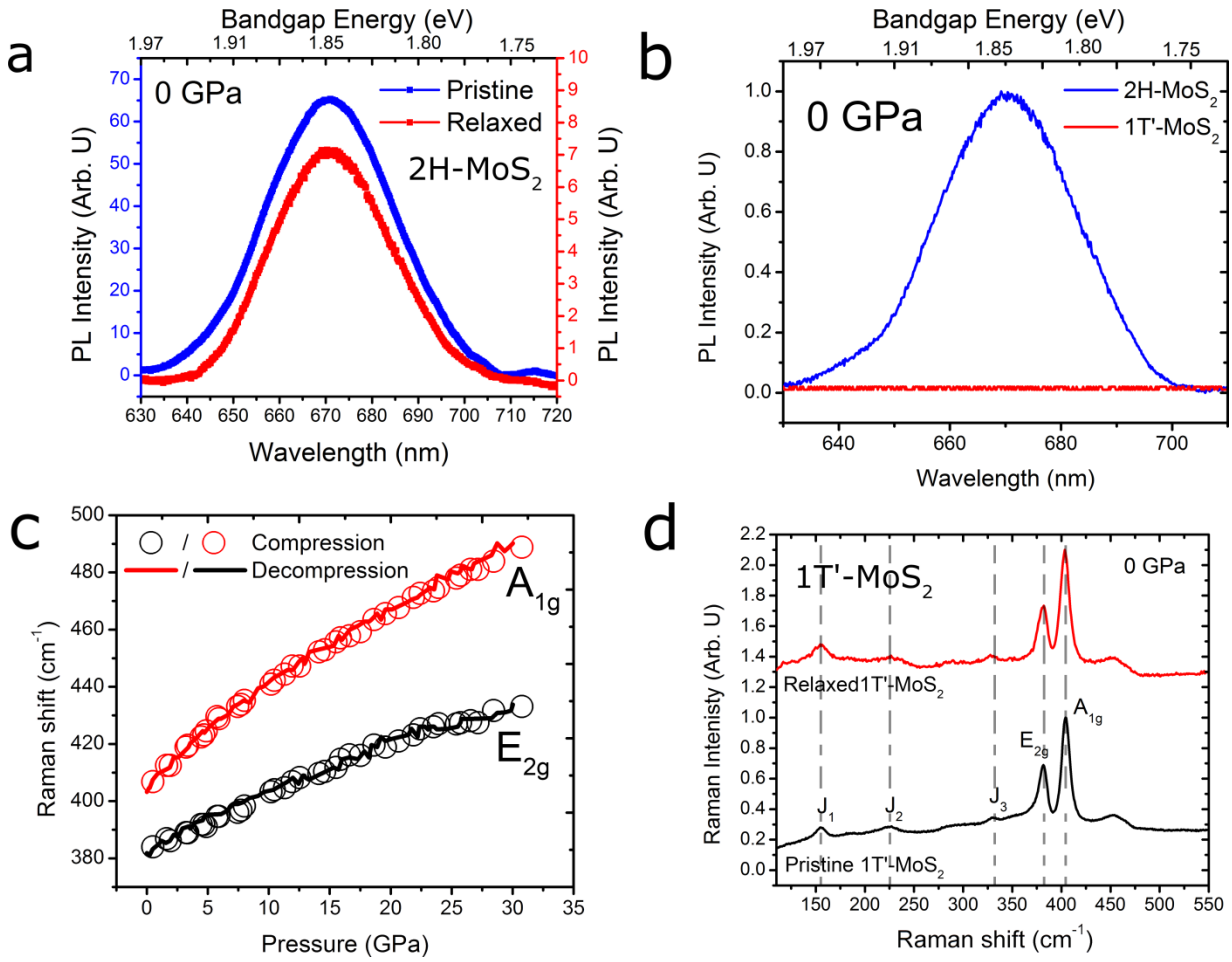

Figure S7. Reversible Pressure Effects on Monolayer MoS_2. (a) PL from monolayer MoS_2 before and after hydrostatic pressure of 30 GPa is applied across the monolayer 2H-MoS_2. **(b)** The PL for the 1T'-MoS_2 and 2H-MoS_2 at 0 GPa. The 1T'-MoS_2 does not show PL behavior. **(c)** Upon decompression, the Raman active A_{1g} and E_{2g} modes compare well with the Raman spectra with increasing pressure, suggesting that the pressure effects are reversible. **(d)** Pristine and relaxed 1T'-MoS_2 show the J_1, J_2, and J_3 active modes, indicating that the pressure effects are reversible.

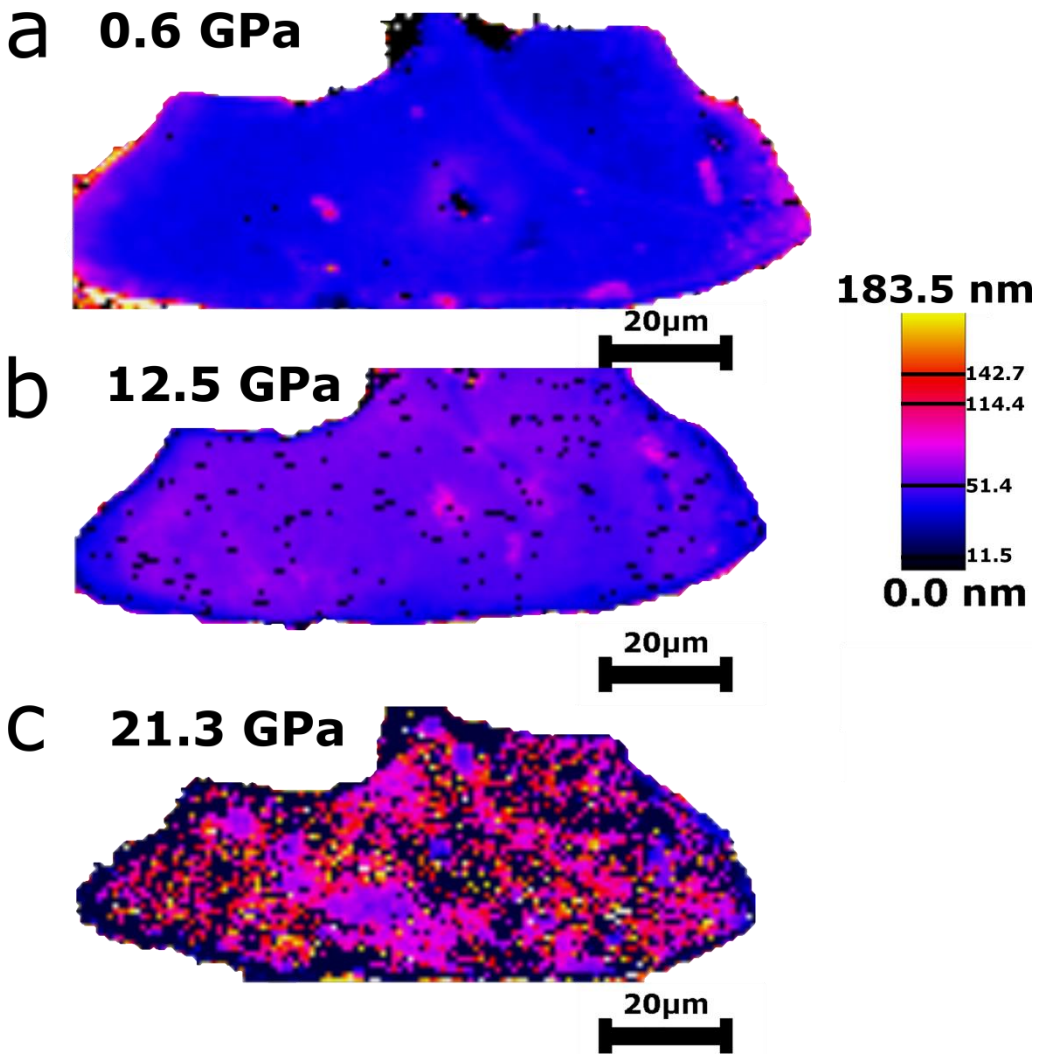

Figure S8. FWHM of the PL Spectra from Monolayer MoS_2. (a) The FWHM map showing an increase with hydrostatic pressure at **(a)** 0.6 GPa **(b)** 12.5 GPa and **(c)** 21.3 GPa the diminishing of the PL peak that suggest the PL at high pressures is unresolvable past 16 GPa at room temperature. The black dots represent where the peaks are diminished into the background noise.

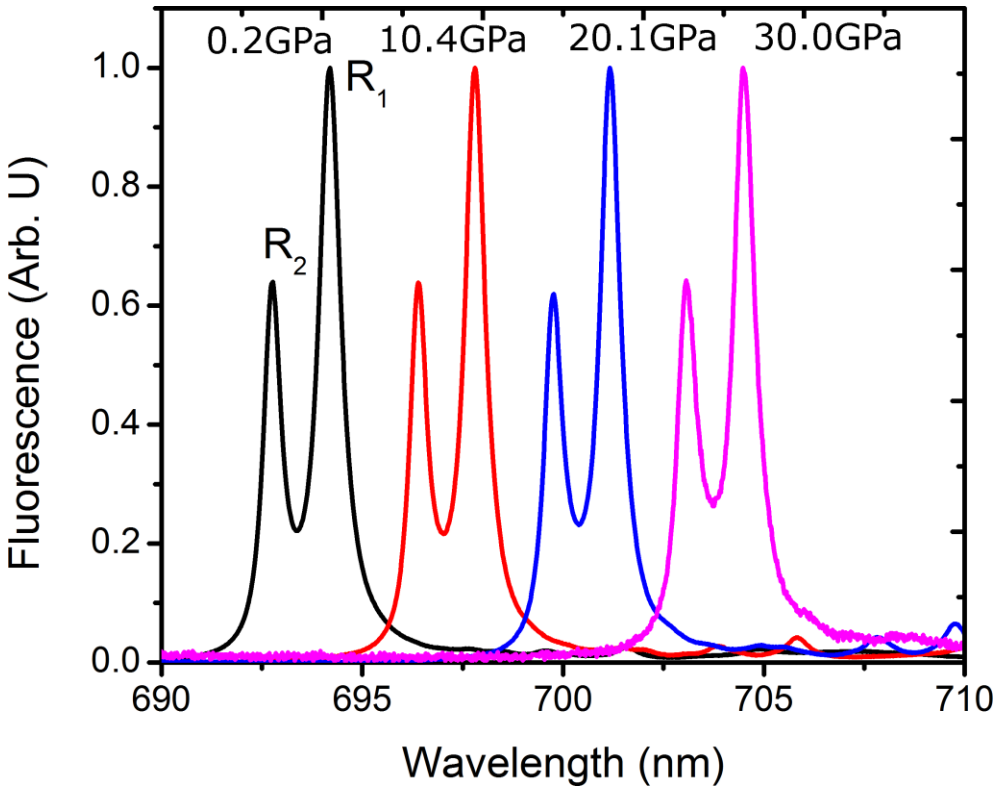

Figure S9. Fluorescence Spectra Shift in Ruby. The R_2 and R_1 ruby luminescence peaks are used to measure the pressure shift. The evolution of the PL spectra from ruby is used as a calibrant to measure the pressure experienced by the sample.

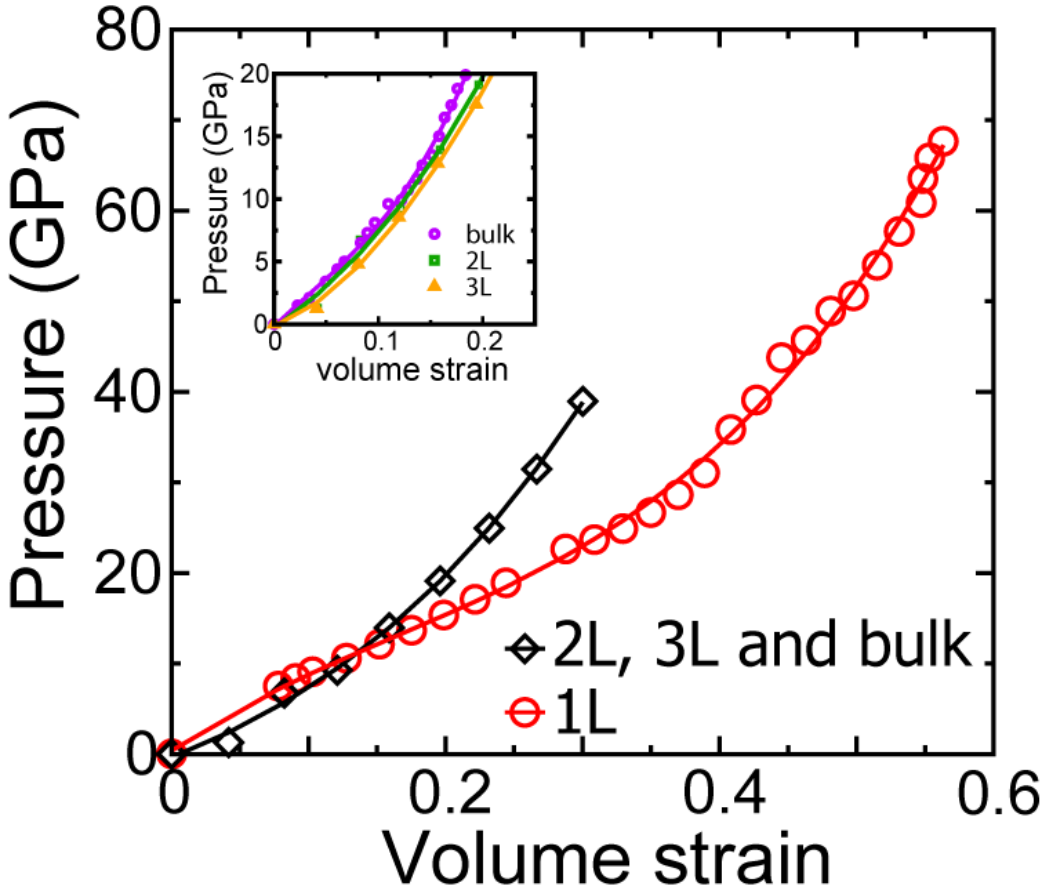

Figure S10. Relation between Volume Strain and Pressure for 2H-MoS_2 Family. 2L, 3L and Bulk follow the same trend and the data can be fitted to a third order polynomial as $P = -0.36 + 59.81\varepsilon + 137.96\varepsilon^2 + 325.93\varepsilon^3$. However 1L depicts a completely different behavior, the polynomial fit of 1L data can be given as $P = 0.39 + 101.24\varepsilon - 220.72\varepsilon^2 + 446.7\varepsilon^3$. These different behaviors arise due to absence of interlayer interaction for monolayer MoS_2. Inset: 2L, 3L and bulk have almost same dependence between volume strain and pressure.

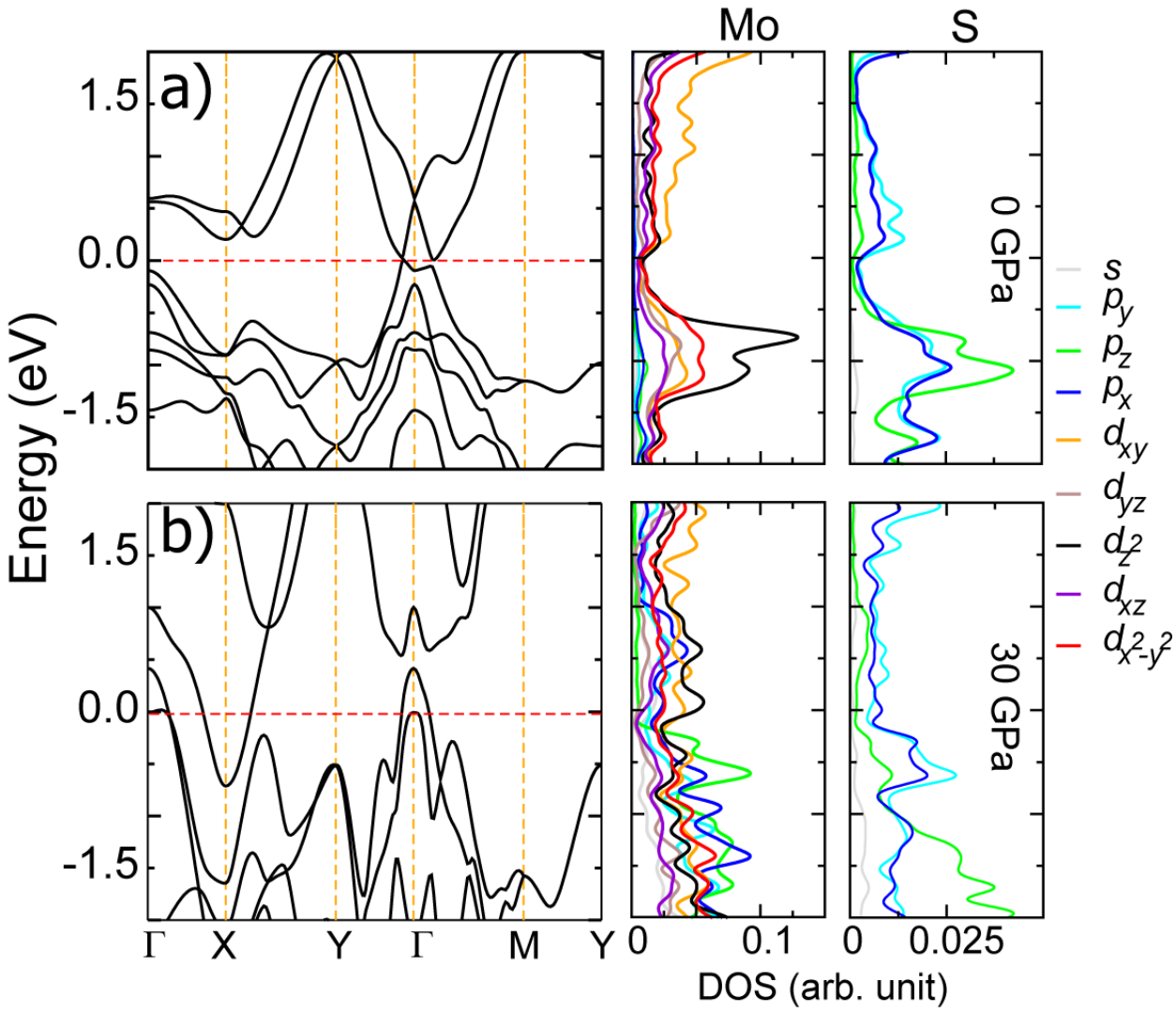

Figure S11. Band Structure and Density of States for the 1T'-MoS_2 Monolayer. (a) At 0 GPa pressure and **(b)** 30 GPa. The monolayer 1T'-MoS_2 is metallic and becomes more metallic under hydrostatic pressure. Upon application of hydrostatic pressure the hybridization between Mo *d*-orbitals (mainly d_{z^2}, d_{xy} and $d_{x^2-y^2}$) and S *p*-orbitals increases, there is an increase in the overlap between conduction and valence bands, increasing the extent of metallization.

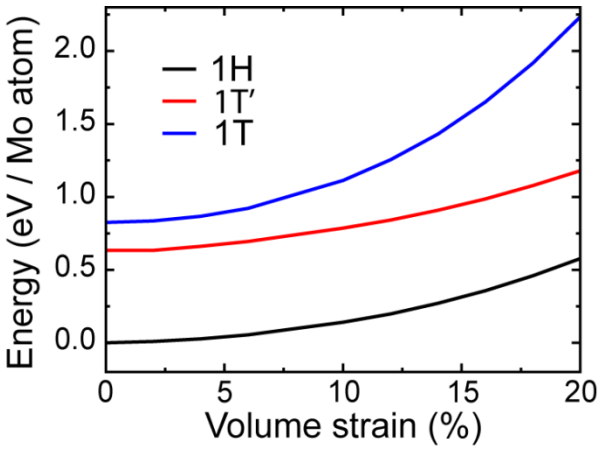

Figure S12. Stability of Different MoS_2 Monolayer Polytypes with Respect to the 2H-MoS_2 Monolayer as a Function of Volume Strain. Monolayer 2H-MoS_2 (i.e. 1H-MoS_2) is the most stable phase at ambient conditions and remains energetically favorable even under high strains. The absence of cross over between the various energy plots indicates the absence of phase transformation between 2H and monolayer 1T'-MoS_2 which is in agreement with our Raman spectra.

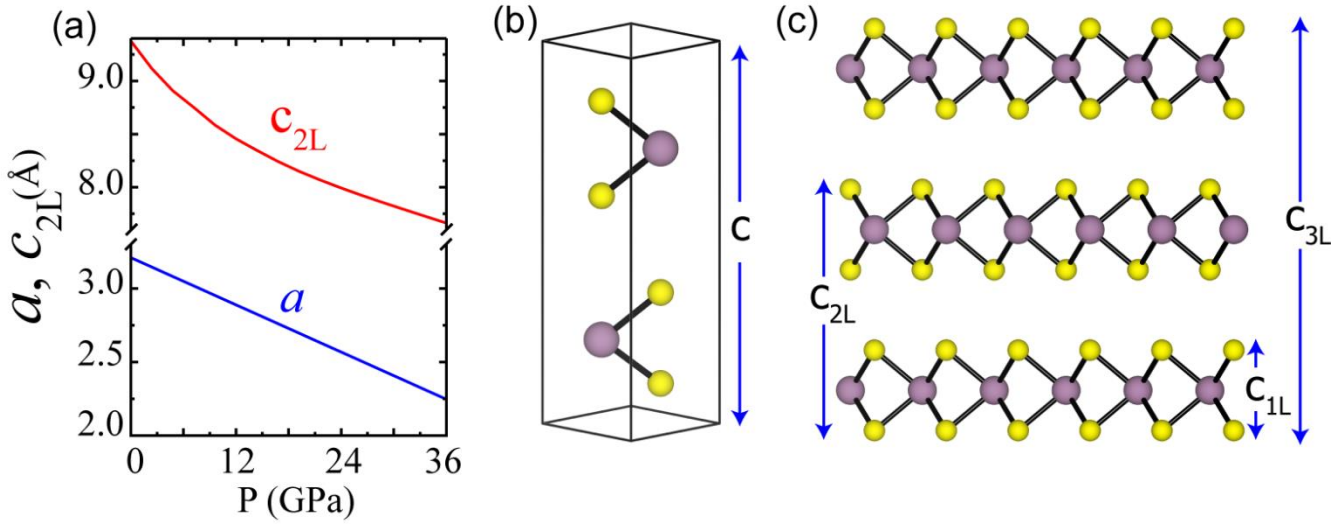

Figure S13. **Compression of the in-plane and out-of plane axis. (a)** Variation in slab thickness (c_{2L}) and in-plane lattice parameter *a* under hydrostatic pressure**.** Illustration of slab thickness for **(b)** bulk and **(c)** 1L, 2L, and 3L MoS_2.